Multiple Injection Strategies for Reducing HC and CO Emissions in Diesel-Methane Dual-Fuel Low Temperature Combustion

*Deivanayagam Hariharan[1,2], Sundar Rajan Krishnan[1], Kalyan Kumar Srinivasan[*1], Aamir Sohail[3]*

[1]Department of Mechanical Engineering, The University of Alabama, Tuscaloosa, AL 35487-0276, USA

[2]Alabama Transportation Institute, The University of Alabama, Tuscaloosa, AL 35487-0276, USA

[3]Ross Business School, University of Michigan 701 Tappan Ave, Ann Arbor, MI 4810

.

ABSTRACT

Dual fuel low temperature combustion (LTC), while promising extremely low engine-out emissions of oxides of nitrogen (NOx) and particulate matter (PM), is beset with high unburned hydrocarbon (HC) and carbon monoxide (CO) emissions, especially at low engine loads. In the present work, diesel dual injection is experimentally shown to achieve simultaneous reduction of HC and CO emissions without compromising NOx and PM benefits.

The motivation to use a second late diesel injection (typically after top dead center (ATDC)) is to oxidize HC arising from incomplete methane oxidation in dual-fuel combustion initiated by the first early diesel injection (around 310 CAD). Since the second diesel injection occurs during the expansion stroke, the NOx-formation propensity is reduced due to low local temperatures. The experimental matrix consisted of twenty-two distinct operating points on a single cylinder research engine (SCRE) adapted for diesel-ignited methane dual fueling. All the

[*] Corresponding Author Email: srini002@ua.edu, T: +1 205 348 6582

experiments were performed at a constant intake pressure of 1.5 bar and fixed first diesel injection timing at 310 CAD whereas, the second diesel injection timing was varied between 320 and 375 CAD and the injection pressure was varied between 500 – 1500 bar. In addition to reductions in ISHC (54%, to 13.7 g/kW-hr), ISCO (46%, to 2.7 g/kW-hr), and ISNOx (7%, to 0.31 g/kW-hr) emissions, a 11% increase in indicated fuel conversion efficiency (IFCE) and a 12% increase in combustion efficiency (η_c) were achieved relative to the baseline single injection (at 310 CAD) dual-fuel LTC. Although smoke emissions increased slightly from 0.03 to 0.06 Filter Smoke Number, they are still considerably lower than for conventional diesel operation.

Keywords. dual fuel; low-temperature combustion; multiple injections; RCCI; natural gas; NO_x emissions

ABBREVIATIONS

AHRR	Apparent Heat Release Rate
ATDC	After Top Dead Center
BDC	Bottom Dead Center
BMEP	Brake Mean Effective Pressure
BTDC	Before Top Dead Center
CA5-90	Crank angle degrees between the locations of 5% and 90% cumulative heat release
CA5	Crank angle at which 5% of cumulative heat release occurs
CA50	Crank angle at which 50% of cumulative heat release occurs
CA90	Crank angle at which 90% of cumulative heat release occurs
CAD	Crank Angle Degrees
CO	Carbon monoxide

48	COV	Coefficient of Variation
49	EGR	Exhaust Gas Recirculation
50	EOI	End of Injection of Diesel
51	FSN	Filter Smoke Number
52	HC	Unburned hydrocarbon
53	ID	Ignition Delay
54	IFCE	Indicated Fuel Conversion Efficiency
55	IMEP	Indicated Mean Effective Pressure
56	LHV	Lower Heating Value
57	LTC	Low-temperature combustion
58	MPRR	Maximum Pressure Rise Rate
59	NOx	Oxides of nitrogen
60	PES	Percent Energy Substitution
61	P_{in}	Intake manifold (boost) pressure
62	P_{rail}	Rail pressure
63	SCRE	Single Cylinder Research Engine
64	SOC	Start of Combustion
65	SOI	Start of Injection of Diesel
66	TDC	Top Dead Center
67	η_c	Combustion Efficiency

1. INTRODUCTION

Advanced low temperature combustion (LTC) concepts exhibit the potential to produce diesel-like efficiency, very low particulate matter (PM) and ISNOx emissions. However, its high CO and unburned hydrocarbon (HC) emissions, especially at low loads is a major stumbling block. Various single fuel LTC strategies such as homogeneous charge compression ignition [1], partially premixed combustion [2, 3], gasoline compression ignition combustion [4, 5], thermally stratified compression ignition [6, 7] and dual fuel LTC strategies [8 – 12] such as reactivity-controlled compression ignition [13 – 15] have been investigated. In the present work, we focus on dual-fuel LTC, whose benefits has been documented extensively for several decades [16 – 27]. In dual fuel LTC, diesel-like high-reactivity fuels are used to ignite a premixed mixture of a low-reactivity fuel such as natural gas (or methane), propane, and gasoline and air. With introduction of the second fuel, we introduce a new degree of freedom, which is the energy or mass ratio between the two fuels. In dual-fuel LTC, it is commonly defined as percentage energy substitution (PES), which is defined as the percentage of high-reactivity fuel energy input substituted by the low-reactivity fuel.

Various researchers have studied the effect of PES [28 – 31] on dual fuel combustion and found that increasing PES lowers NOx and soot emissions. This can also be explained based on Dec's conceptual model of diesel combustion [32], where he found that soot emissions are formed primarily in the rich premixed regions of the diesel jet, and NOx emissions were formed in the high-temperature diffusion flame enveloping the diesel jet. In dual fuel combustion, by increasing the PES, the diesel jet's size is reduced. The resulting NOx emissions are much lower since NOx emissions scale with diesel quantity and the corresponding size of the diffusion flame (if it exists) enveloping the diesel jet. Additionally, the predominantly lean methane-air combustion results in

reduced soot emissions. Along with the PES, the effect of other control parameters such as fuel injection pressure, SOI, and intake air pressure and temperature on dual fuel combustion were investigated by Krishnan et al., [28]. They report NOx and HC emissions trade-off, showing a drop in NOx emissions with increase in HC emissions as the diesel SOI is advanced (300 CAD). This is mainly due to the dual-fuel combustion being a mixing based combustion technique, as the SOI is advanced, the high reactivity fuel gets more time to mix and resulted in less rich regions and retards the combustion phasing.

Previous research from the same engine setup by Raihan et.al., [33] and Guerry et.al., [34] has demonstrated significant NOx benefits and IFCE benefits by advancing the diesel SOI up to 300 CAD. In addition, Raihan et.al., [33] showed that lower injection pressures result in more heterogeneous fuel-air mixtures, causing higher ISNOx and ISHC emissions. Guerry et.al., [34] has shown increase in ISCO and ISHC emissions for diesel SOI earlier than 300 CAD. In the current study we examine the advantages of a dual injection strategy in minimizing engine-out emissions and improving fuel conversion efficiencies in diesel-methane dual fuel combustion. Carlucci et al., [35] showed splitting pilot injection increases fuel conversion efficiency and reduce emissions, especially at low loads using biogas-bio diesel. Following that other researchers showed similar results with various fuel combinations butanol-diesel [36, 37], natural-gas-diesel [38, 39], and gasoline-diesel [40]. In this context, the current study uses methane-diesel fuel combination with earlier pilot injection (310 CAD) of diesel, the effect of splitting the pilot injection, the effect of dwell between the two injections, and the effect of fuel injection pressures on IFCE and engine out emissions were discussed to determine the best operating condition at 5 bar brake mean effective pressure (BMEP).

OBJECTIVE

The objective of the present work is to minimize the ISHC and ISCO emissions and improve combustion efficiency with minimal impact on ISNOx emissions in dual fuel LTC by introducing a second injection of diesel. At a fixed intake pressure of 1.5 bar, engine speed of 1500 rpm, and fixed first diesel SOI of 310 CAD, the effect of the second diesel SOI, injection duration, PES, and rail pressure (Prail) on the engine performance, combustion, and exhaust emissions were investigated in a single cylinder research engine (SCRE).

2. EXPERIMENTAL SETUP

The layout of the experimental test cell is shown in Figure 1. The SCRE details are shown in Table 1. A 250 HP AC regenerative dynamometer (Dyne Systems), controlled by an Interloc V engine controller, coupled to the SCRE was used both to motor the engine and also to measure the torque and the speed of the engine. An integrated emissions bench (Altech Environment) was used to measure engine-out total HC, NO_x, CO, CO_2, and O_2 emissions. The bench was calibrated using known concentrations of the same gases (except for HC, for which propane was used). The calibration gas concentrations are shown in Table 2. A sample trolley equipped with a heated pump and heated lines maintained at 191±5°C to prevent condensation of the HC before reaching the emissions bench. Smoke was measured using an AVL 415S variable sampling smoke meter in Filter Smoke Number (FSN). The emissions were computed as an average of data recorded for 60 seconds and converted to indicated-specific units using SAE J1003 standard [41].

Table 1: Engine Specifications

Engine Type	Rsi-130 Doosan DV-11 SCRE
Displacement Volume	1.827 liters

Compression Ratio	17.1:1
Maximum Engine Speed	1900 RPM
Bore x Stroke	128 x 142 (mm x mm)
Connecting rod length	228 mm
Valve Train	2 Intake, 2 Exhaust valves
Intake valve open (CAD absolute)	32º
Intake valve close (CAD absolute)	198º
Exhaust valve open (CAD absolute)	532º
Exhaust valve close (CAD absolute)	14º
Diesel Injection System	CP3 Pump, Common rail
Injector nozzle hole diameter	0.197 mm
Number of nozzle holes	8

Diesel injection in the cylinder was achieved using a Stand-Alone Diesel Injector (SADI) controller from National Instruments. A Bosch CP3 common-rail fuel injection pump and injector were employed. Crank-resolved injector needle lift was measured using a Hall effect sensor. Ultra-Low Sulfur Diesel (Sulfur 15 ppm, cetane number CN40 minimum) fuel and methane (Ultra high purity 99.97 %,) were used for fueling the engine. Methane fumigation in the air intake manifold was controlled by a current-controlled electronic valve (HANBAY Model MCM-050AB). The flow rates of diesel and methane were monitored using Coriolis flowmeters (MicroMotion Model CMF025M319N2BAEZZZ).

The diesel fuel was cooled by a fuel heat exchanger. In-cylinder pressure was monitored using a Kistler 6052C pressure transducer and a Kistler 5010B charge amplifier. The pressure transducer was mounted flush with the inner periphery of the cylinder head to avoid any pipe oscillations. An AVL Indismart data acquisition system collected the cylinder pressure and needle lift data over 1000 cycles. Other calculated parameters, including maximum pressure rise rate

(MPRR), coefficient of variation (COV) of indicated mean effective pressure (IMEP), ignition delay, combustion phasing (CA50), and IMEP were also ensemble-averaged over 1000 cycles. A shaft encoder with a resolution of 0.1 crank angle degrees (CAD) was connected to the engine crankshaft to trigger cylinder pressure data acquisition. The encoder TDC and the physical engine TDC were software phased to ensure crossover-free motoring pressure traces. In-cylinder pressure was pegged to the intake manifold pressure at BDC using an intake manifold absolute pressure sensor.

K-type thermocouples were used for temperature measurements. Engine Oil Temperature Conditioner (EOTC) and Engine Water Temperature Conditioner (EWTC) with PID control loops maintained the engine oil and coolant water temperatures, respectively, at 80 °C. An air compressor coupled with a heatless desiccant dryer was used to simulate intake air boost. A sonic orifice flowmeter (Model SN16–SA–235) measured the intake air mass by ensuring choked flow across its orifice and recording the upstream pressure and temperature. Accuracies of experimental measurements are listed in Table 2.

Table 2: Accuracies of Experimental Measurements

Measured parameter	Unit	Concentration	Accuracy
Engine Speed	RPM	N/A	± 1 rpm of reading
Engine Torque	Nm	N/A	± 0.06% of reading
Cylinder pressure	bar	N/A	± 0.005 of reading
Diesel flow rate	kg/h	N/A	± 0.05% of reading
Methane flow rate	kg/h	N/A	± 0.35% of reading
Airflow rate	kg/h	N/A	± 0.1% of reading
Temperatures	°C	N/A	± 0.75% of reading
Pressures (intake, exhaust, coolant, and lubricating oil)	psig	N/A	± 0.25% of reading

Smoke number	FSN	N/A	± 0.001% of reading
THC emissions	ppm	8688 ppm	<0.5% of the full scale
NOx emissions	ppm	2006 ppm	<1% of the full scale
CO emissions	%	8%	<1% of the full scale
CO_2 emissions	%	18%	<1% of the full scale
O_2 emissions	%	17%	<1% of the full scale

2.1 Experimental Matrix

The experimental matrix consisted of 22 operating points (OP#) and their details are provided in

Table 3. Additional details of this experimental matrix can be found Sohail [42]. The first operating point, OP#1, is considered the baseline. Baseline corresponds to diesel-methane dual fuel LTC with single diesel injection, at 85 PES. The baseline point was recorded at the constant engine operating parameter values of 1500 rpm, Pin = 1.5 bar, Tin = 35 deg C and producing 5 bar BMEP. Diesel fuel rail pressure was maintained at 500 bar and the SOI was fixed at 310 CAD, with no external EGR. As mentioned earlier, an additional injection of diesel was introduced starting from the second operating point, OP#2, to quantify its effect on decreasing HC and CO emissions as well as on η_c and IFCE. For OP#2 and OP#3, the second injection was tried at 320 CAD and 325 CAD, to see the effect of close-coupled injections.

However, due to the adverse effect of OP#2 and OP#3 on ISNOx emissions, the second SOI was delayed beyond TDC to 370 CAD and 375 CAD for OP#4 and OP#5, respectively, while decreasing the PES to 75%. The second SOI of 375 CAD at 75 PES showed improvements in ISNOx emissions compared to closed couple injections. However, even with OP#4 and OP#5, IFCE and smoke emissions were compromised and therefore, from OP#6 onward, all other parameters were kept constant, and only the injection pressure was increased along with appropriate adjustments to the injection duration to maintain a constant BMEP.

Table 3: Experimental Test Matrix

OP#	PES	First SOI	Inj Dur1	Second SOI	Inj Dur2	Injection Pressure
-	%	CAD	ms	CAD	ms	bar
1	85	310	0.52	-	-	500
2	85	310	0.425	320	0.425	500
3	85	310	0.436	325	0.436	500
4	75	310	0.52	370	0.42	500
5	75	310	0.52	375	0.49	500
6	75	310	0.52	375	0.465	550
7	75	310	0.52	375	0.35	600
8	75	310	0.52	375	0.31	650
9	75	310	0.52	375	0.192	700
10	75	310	0.5	375	0.29	700
11	75	310	0.49	375	0.31	700
12	75	310	0.45	375	0.29	800
13	75	310	0.46	375	0.265	800
14	75	310	0.42	375	0.28	900
15	75	310	0.46	375	0.17	900
16	75	310	0.45	375	0.135	1000
17	75	310	0.405	375	0.257	1000
18	75	310	0.39	375	0.25	1100
19	75	310	0.385	375	0.255	1200
20	75	310	0.36	375	0.275	1300
21	75	310	0.325	375	0.295	1400
22	75	310	0.325	375	0.32	1500

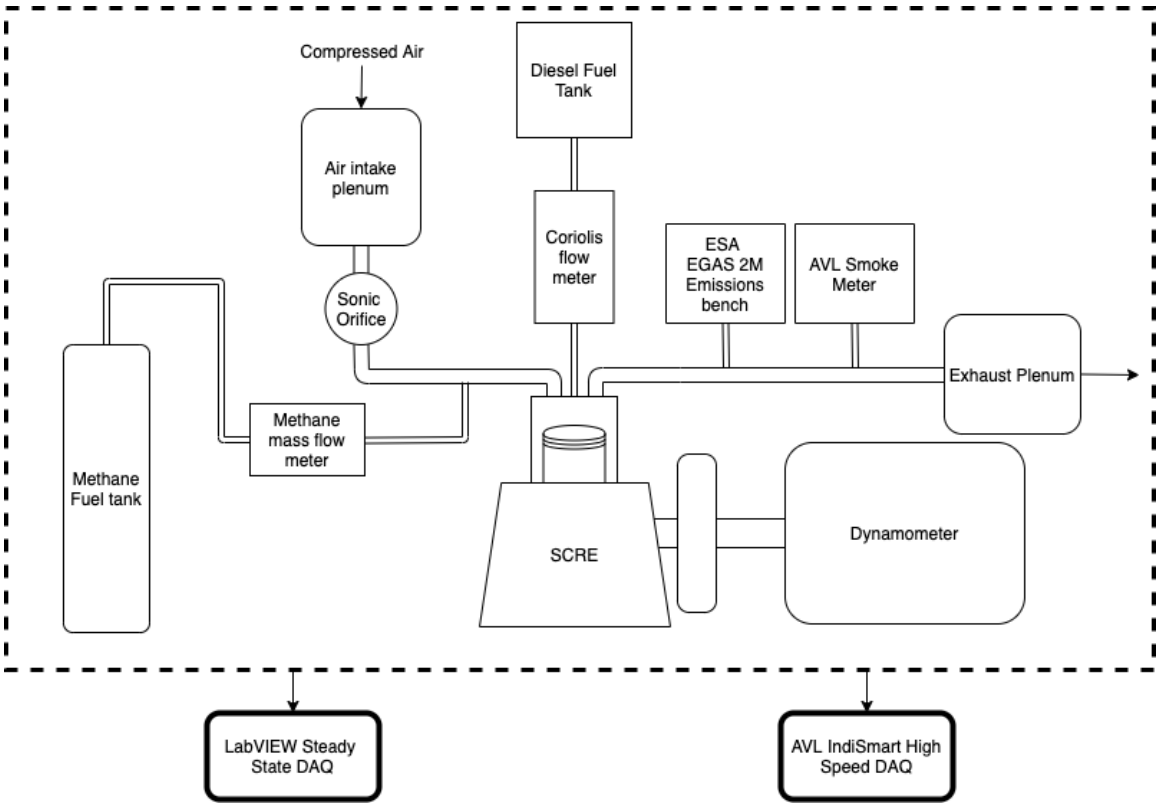

Figure 1: Experimental setup of the single-cylinder research engine

2.2 Definitions

Important parameters used in this paper such as the overall equivalence ratio (Φ), percent energy substitution (PES), ignition delay (ID), combustion efficiency (η_c), and net apparent heat release rate (AHRR) are defined below:

$$PES = \frac{\dot{m}_g LHV_g}{\dot{m}_d LHV_d + \dot{m}_g LHV_g} \times 100\% \quad (1)$$

$$\Phi = \frac{\left(A/F\right)_{st-tot}}{\left(\frac{\dot{m}_a}{\dot{m}_d + \dot{m}_g}\right)} \quad (2)$$

$$ID = CA5 - SOI \quad (3)$$

$$\eta_c = 1 - \frac{\sum_i x_i Q_{LHVi}}{\left(\frac{\dot{m}_f}{\dot{m}_f + \dot{m}_a}\right) Q_{LHVf}} \quad (4)$$

$$AHRR(\theta) = \frac{\gamma}{\gamma - 1} P \frac{dV}{d\theta} + \frac{1}{\gamma - 1} V \frac{dP}{d\theta} \quad (5)$$

In Equations 1 and 2, $\dot{m}$ refers to the mass flow rates of diesel (subscript *d*), gaseous methane fuel (subscript *g*), and air (subscript *a*), and LHV refers to the corresponding fuel lower heating values. Stoichiometric air-fuel ratio $(A/F)_{st\text{-}tot}$ is defined as the stoichiometric air required for complete oxidation of both diesel and methane into CO_2 and H_2O. Therefore, $(A/F)_{st\text{-}tot}$ is dependent on the PES of methane. In Equation 3, the ignition delay is defined as the time elapsed from SOI to start of combustion (SOC), which is defined as the crank angle at which 5% of cumulative heat release occurs (CA5). Similarly, combustion phasing (CA50) and combustion duration (CA5-90) are defined as the crank angle at which 50% of cumulative heat release occurs and the difference between the 5% and 90% cumulative heat release crank angles, respectively.

In Equation 4, combustion efficiency (η_c) is calculated using the mass fractions (x_i) of CO, H_2, HC, and PM using their respective LHVs (Q_{LHV_i}) [43]. In this study, only the measured CO and HC concentrations and the H_2 mass fractions estimated from stoichiometry calculations are used in the η_c calculations. Since the composition of HC in the exhaust, and thus its LHV, are not known, Heywood [43] recommends using the LHV of the fuel as they are expected to be of comparable magnitude. However, since two fuels are used for dual fuel combustion, the exhaust HC can theoretically originate from both fuels; therefore, the combined mass-fraction-weighted LHV of diesel and methane is used to represent the LHV of HC. The lower heating values for methane, CO, and H_2 are assumed to be 50 MJ/kg, 10.1 MJ/kg, and 120 MJ/kg, respectively. Also,

since gravimetric PM was not measured in the present experiments, it was not considered in the η_c calculations.

The net AHRR was derived from measured in-cylinder pressure data using Equation 5. The instantaneous volume (V) was calculated from the engine geometry and derivatives of pressure and volume ($dP/d\theta$ and $dV/d\theta$) were calculated numerically using a four-point central difference formula. The specific heat ratio (γ) required in Eq. 5 was evaluated using an in-house MATLAB based chemical equilibrium code, which uses the real gas temperature (Redlich–Kwong equation of state) and NASA polynomials [44] as basic inputs.

3. RESULTS AND DISCUSSION

In this section, combustion, performance, and emissions results for single- and dual-injection diesel-methane LTC are presented and efficiency-emissions tradeoffs are discussed based on results obtained at the 22 different operating points.

3.1 Effects of SOI of Second Diesel Injection

In this section, we focus on the first five operating points in Table 3. Starting with OP#1, which involves a single diesel injection at 85 PES, followed by a close-coupled second diesel injection, which corresponds to OP#2 and OP#3, and finally for the last two points (OP#4 and OP#5) the second injection occurs after TDC, with PES reduced to 75%.

3.1.1 Crank-Resolved Apparent Heat Release Rate and Cylinder Pressure

Figure 2 illustrates the cylinder pressure and injector needle lift profiles and Figure 3 shows the AHRR of the aforementioned five cases (OP#1 to OP#5). Additionally, CA5, CA50, and CA90 are also marked on the cylinder pressure traces in Figure 2 for reference. Considering the baseline

(OP#1 with single injection), OP#2 and OP#3 have significantly earlier CA5 due to the high stratification of the fuel-air mixture caused by the second injection. This also advances the combustion phasing (CA50) to before TDC, which results in a higher peak cylinder pressure than the single injection baseline case (OP#1). For OP#2 and OP#3, the second SOIs of 320 CAD and 330 CAD, respectively, can be seen clearly from the needle lift curves. To maintain constant BMEP (5 bar) and constant injection pressure of 500 bar, the first injection duration had to be decreased with the introduction of the second injection. It can also be seen from Figure 2 that the peak needle lift of the first injection dropped with injection duration for these two cases.

However, OP#4 and OP#5 were able to simultaneously maintain the 5 bar BMEP along with the same first injection duration and needle lift as the baseline OP#1. This was achieved by retarding the second injection well past the CA50. It can also be seen from Table 3 that the first injection duration of OP#1, OP#4, and OP#5 are all the same. In the absence of additional diesel fuel from the second injection before CA5, the SOC of OP#4 and OP#5 were delayed compared to OP#2 and OP#3. However due to slight decreases in the methane flow rate (PES decreased from 85% and 75%) in OP#4 and OP#5 from the baseline resulted in slightly delayed CA50.

From Figure 2, it can be seen that by retarding the second SOI to 370 CAD and 375 CAD and reducing the PES at constant BMEP, the combustion phasing is retarded to almost same as that of the baseline (OP#1). Another important reason behind the delayed SOC and CA50 for OP#4 and OP#5 is that they have the same amount of diesel at SOC but less methane compared to the baseline (OP#1). From Table 3, it can be noticed that the SOI of the first injection (which contributes to the SOC), the injection pressure, and the injection duration for OP#4 and OP#5 are the same as those for OP#1, but with 75 PES, instead of 85 PES. This reduction in PES, while

keeping the first diesel injection amount constant implies lower ambient methane concentration (everything else remaining the same), and therefore, lower peak cylinder pressure for OP#4 and OP#5, compared to OP#1.

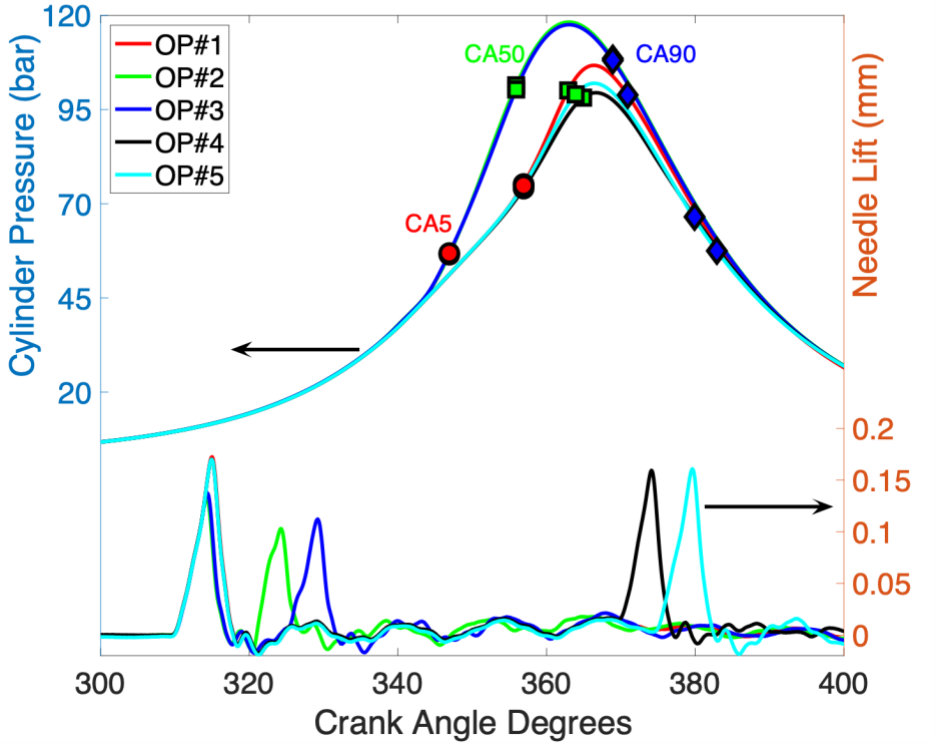

Figure 2: Cylinder pressure and needle lift histories at a constant speed of 1500 rpm, intake pressure of 1.5 bar, and a fuel injection pressure of 500 bar, over a range of SOI as described in

Table 3; Their corresponding CA5 (circles), CA50 (squares), and CA90 (diamonds) were also plotted on top of the cylinder pressure trace.

The apparent heat release rate (AHRR) trends for OP#1 through OP#5 are shown in Figure 3. The baseline case (OP#1) exhibited the highest peak AHRR of ~200 J/CAD. The earlier combustion phasing of OP#2 and OP#3 are due to their close-coupled dual injection, that results in shorter ignition delays (in fact, less than 20 CAD after the second injection near 320-325 CAD) with more stratified mixtures. This leads to higher LTHR peaks, and consequently, earlier HTHR. Since the initial combustion process is more stratified for OP#2 and OP#3, the peak AHRR are lower compared to OP#1, 4, and 5. OP#4 and OP#5 have similar peak heat release rates and their CA50 is very similar to that of the baseline OP#1. However, they have a secondary heat release rate caused by the second injection. This secondary heat release close to the end of the main heat release for OP#4 and OP#5, extends the combustion duration and shifts the CA90 significantly later (~378 CAD) than the baseline case (~370 CAD), at a comparable CA50 (~363 CAD).

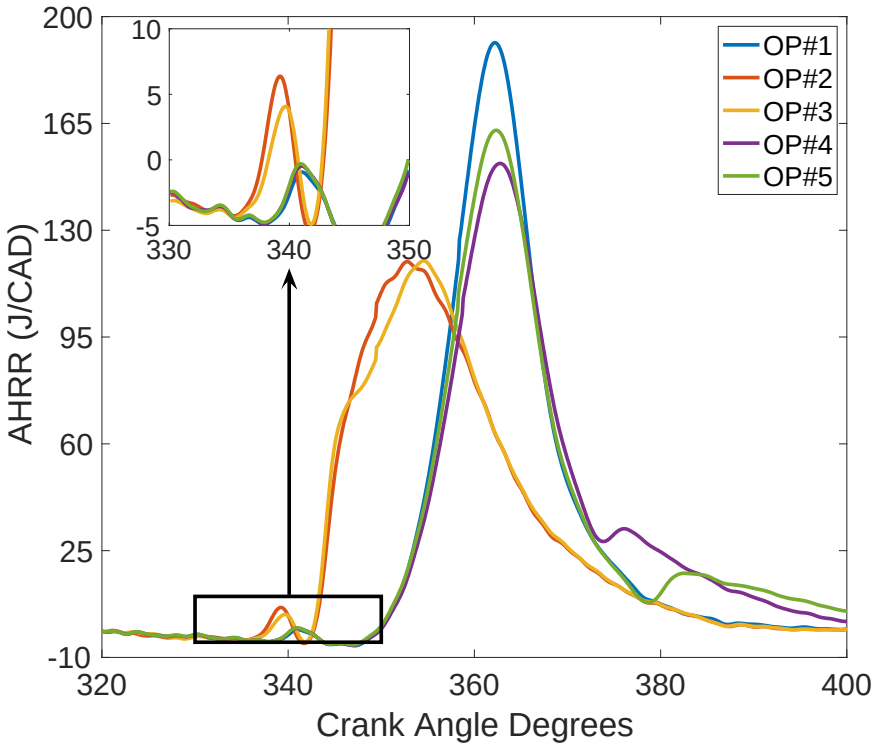

272

273 Figure 3: Apparent heat release rate (AHRR) histories at a constant speed of 1500 rpm,

274 intake pressure of 1.5 bar, and a fuel injection pressure of 500 bar for OP#1 through OP#5 in

Table 3

3.1.2 Efficiencies and Emissions

The indicated fuel conversion efficiencies ($IFCE$) for the first five operating conditions, shown in Figure 4, are very similar, irrespective of the PES or SOI. This is due to the apparent balance between fueling rate requirements, PES, and AHRR behavior across these operating points. The combustion efficiencies (η_c) for all these five points are also shown in Figure 4. Clearly, η_c depends on the CO and HC emissions, which account for partially burned or unburned (mostly methane) fuel in the exhaust. The indicated thermal efficiency (η_{ITE}) should be inversely related to the η_c since the IFCE remains nearly invariant and since the thermal, fuel conversion and combustion efficiencies are related by $IFCE = \eta_c$ x η_{ITE}. So, η_c is significantly better for OP#2 and OP#3, due to their early CA50, which helps with better CO and HC oxidation due to higher in-cylinder temperatures. As CA50 retards, the η_c decreases due to slower oxidation resulting from lower in-cylinder temperatures.

The earlier combustion phasing has a positive impact on the CO and HC emissions but ISNOx emissions are adversely affected as shown in Figure 4(b). For OP#2 and OP#3, ISNOx emissions are significantly higher (more than six times) compared to the other three cases. This is due to the significantly higher local in-cylinder temperatures caused by the earlier combustion phasing at these operating points. By retarding the combustion phasing, ISNOx emissions can be reduced to baseline OP#1 values, albeit, at the expense of soot emissions. Figure 4(a) shows engine-out smoke emissions reported in FSN. With retarded SOIs, ISNOx can be decreased (by approximately 96% from OP#3 to OP#5), as the combustion phasing is retarded. However, with the injection pressure of 500 bar, when the second diesel injection occurs after TDC (during the

297 combustion process), it appears to result in fuel-rich pockets, causing the soot emissions to increase
298 (by approximately 17 times from OP#3 to OP#5).

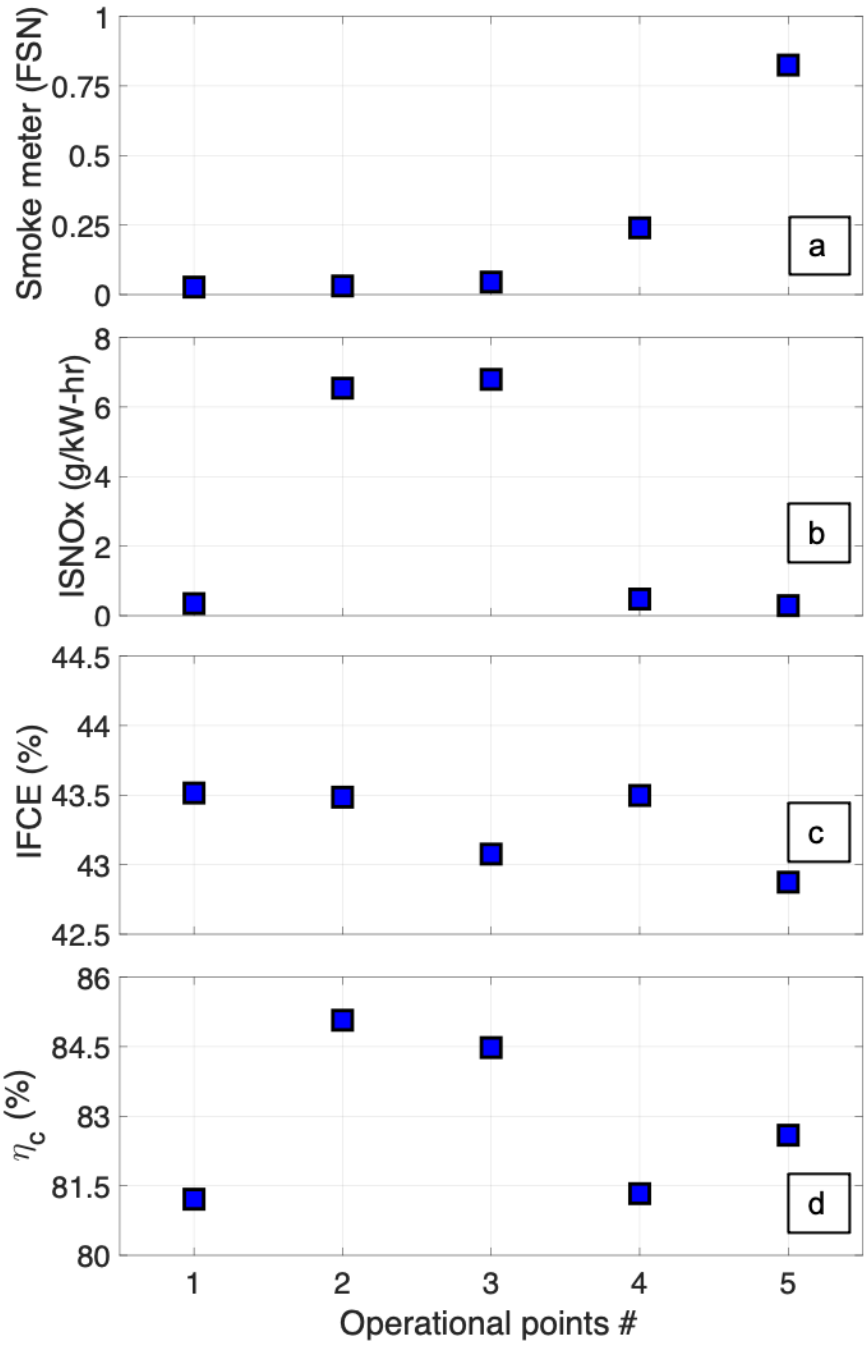

299

300 Figure 4: a) Soot Emissions, b) Indicated specific NOx emissions, c) Indicated fuel
301 conversion efficiency (IFCE), and d) combustion efficiency at a constant speed of 1500 rpm, intake
302 pressure of 1.5 bar, and a fuel injection pressure of 500 bar, over a range of SOI as described in

Table 3

The aforementioned observations indicate that close-coupled injection (OP#2 and OP#3) results in significantly earlier combustion phasing and higher ISNOx emissions relative to OP#1. On the other hand, OP#4 and OP#5 show similar IFCE, η_c, and ISNOx emissions compared to OP#1, however with significantly higher smoke emissions. These results raised a fundamental question: "*Does the double injection strategy not provide reduced CO and HC emissions for dual fuel LTC at 5 bar BMEP without a huge smoke penalty?"* To address this question, the effect of injection (rail) pressure (P_{inj}) was studied. Various researchers have shown the advantages of using high injection pressure in mitigating soot emissions in conventional diesel combustion [45 – 48]. Taking cue from these studies, the same concept was applied to subsequent operating conditions in the current dual fuel LTC experiments.

3.2 Effect of the injection pressure (P_{rail}) and the duration of the injection

This section focuses on the remaining 17 operating points in Table 3. Starting from OP#6 to OP#22, the fuel injection pressure was increased from 500 bar to 1500 bar, keeping the following parameters constant: intake pressure of 1.5 bar, speed of 1500 rpm, PES of 75%, first and second SOIs of 310 CAD and 375 CAD, respectively, and a nominal BMEP of 5 bar.

3.2.1 Apparent Heat Release Rate and Cylinder Pressure

Figure 5 shows the cylinder pressure and needle lift histories for five representative operating points out of all seventeen cases (OP#6 – OP#22) along with the baseline OP#1. To make the plot easy to comprehend, only 5 (OP# 6, 10, 14, 18, and 22) out of 17 operating points are shown along with OP#1 for brevity. Similarly, the AHRR of these six cases are shown in Figure

6. Additionally, CA5, CA50, and CA90 were also marked on the cylinder pressure traces in Figure 5 for reference.

No variations are seen in the cylinder pressure traces across all the six cases up to ~340 CAD, but beyond that, OP#10 showed slightly higher in-cylinder pressure compared to others. It can also be noticed from Figure 5, that OP#10 has the highest peak on the needle lift and it was the latest point to reach zero needle lift, during the first injection of diesel. Despite nearly invariant needle lift profiles and durations, with the fuel rail pressure changing across these six-operating conditions, the total diesel injected amount varied. However, OP#10 had the shortest ignition delay (earliest SOC) and earliest CA50, which leads to the highest peak cylinder pressure. As CA50 is retarded, the peak cylinder pressure decreases, with the OP#22 (the case with highest injection pressure) having the latest combustion phasing and the lowest peak cylinder pressure. Most importantly, the second injection of diesel occurs after CA90 for most of the cases, except for three cases (OP#5, OP#21, and OP#22). So, for most of the cases the second injection of diesel does not have a significant impact on CA50 and contributes less than 10 percent of the overall cumulative heat release.

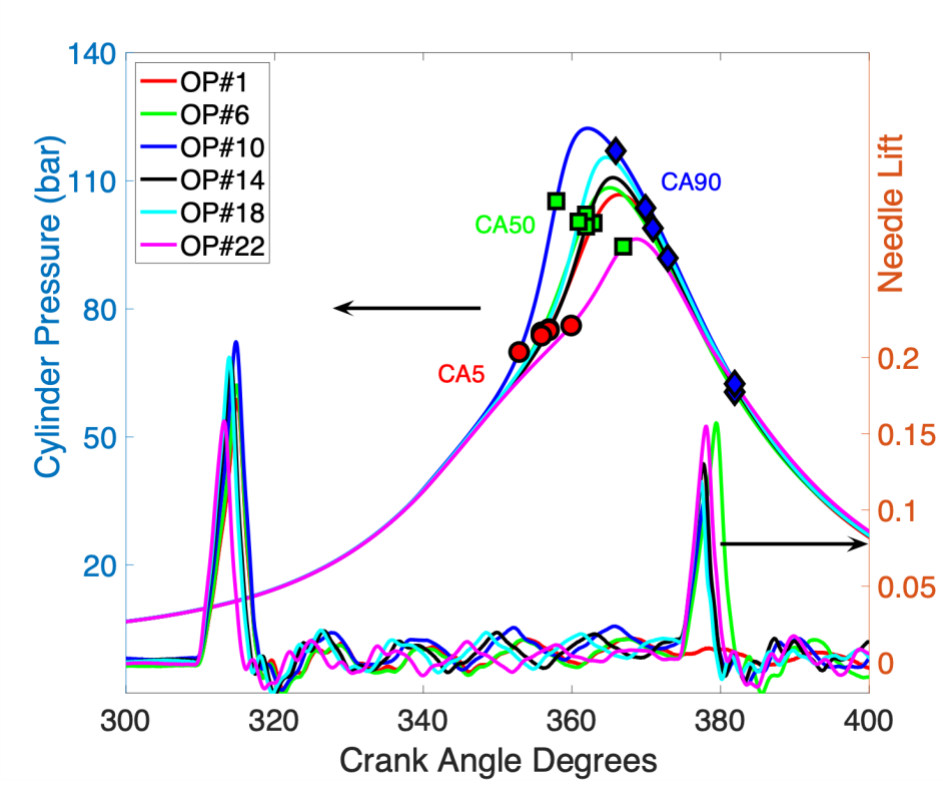

Figure 5: Cylinder pressure and needle lift histories at a constant speed of 1500 rpm, intake pressure of 1.5 bar, and an SOI of 310 CAD and 375 CAD, over a range of fuel injection pressure as described in Table 3

The AHRR trend in Figure 6 shows OP#10 has the highest (~300 J/CAD) and earliest peak heat release. OP#18 also has a very similar heat release rate profile, but with a later combustion phasing, as the peak AHRR occurs after TDC. OP#6 and OP#22 have similar AHRR profiles compared to OP#1, albeit with different combustion phasing. It is important to note that with the change in combustion phasing, the percentage of energy released being converted into useful work varies. Additionally, all the cases with the second diesel injection have a secondary heat release rate after 375 CAD (start of the second injection). To analyze this second heat release rate profile across various cases, a magnified view of the AHRR due to the second injection is showed as an inset plot in Figure 6.

From the inset plot of Figure 6, OP#22 has the highest second peak of ~40 J/CAD at 380 CAD (5 degrees from start of second injection). OP#6 shows a lower second AHRR peak of ~17 J/CAD for an extended duration (even after 385 CAD). The remaining three cases have sharp and short second AHRR peaks since the first AHRR peaks were higher compared to OP#1. The variations in second AHRR depend on the combustion phasing of the first/main heat release and on the mass of fuel injected in the second injection.

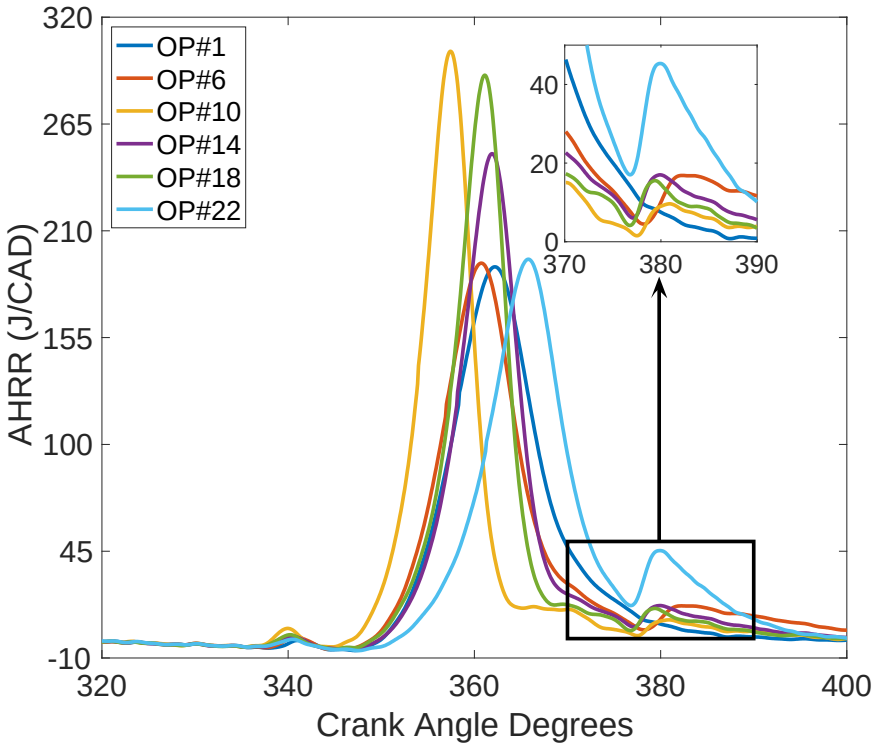

Figure 6: Apparent heat release rate histories at a constant speed of 1500 rpm, intake pressure of 1.5 bar, and an SOI of 310 CAD and 375 CAD, over a range of fuel injection pressure as described in Table 3

3.2.2 Ignition and Combustion Parameters

While a brief picture of the CA5, CA50, and CA90 trends at different fuel injection pressures was provided in Figure 5, in Figure 7, the same trends for all the 17 operating points

(OP#6 to OP#22) are shown along with results for the baseline OP#1 (shown as a dotted line). As expected, with increasing injection pressure, the injection duration is decreased to maintain constant BMEP across these cases. The overall combustion process gets retarded as the duration of the first injection decreases (as fuel injection pressure increases). Additionally, the effect of increasing injection pressure (from 550 bar to 700 bar) at constant first injection duration of 0.52 ms can be seen across the first four points. Among OP# 6 through OP# 9, the mass of fuel injected with the first injection likely increased, based on the following considerations: 1) the constant injection duration with increasing injection pressure and 2) shorter second injection durations (cf. Table 3) to maintain constant BMEP, especially since the overall diesel mass flow rate remained nearly invariant for these OPs.

All OPs except OP#21 and OP#22, have earlier CA5 (start of combustion) and CA50 than the baseline OP#1 due to higher injection pressures. Even though OP#21 and OP#22 have the highest injection pressures, their first injection durations decreased significantly due to longer second injection durations (*cf.* Table 3). The CA90 trends are similar to the CA50 trends in that CA90 retards along with CA50, and vice versa. However, for OP#21 and OP#22, where the second injection produced significant energy output and further retarded CA90, the CA90 occurs after the second injection.

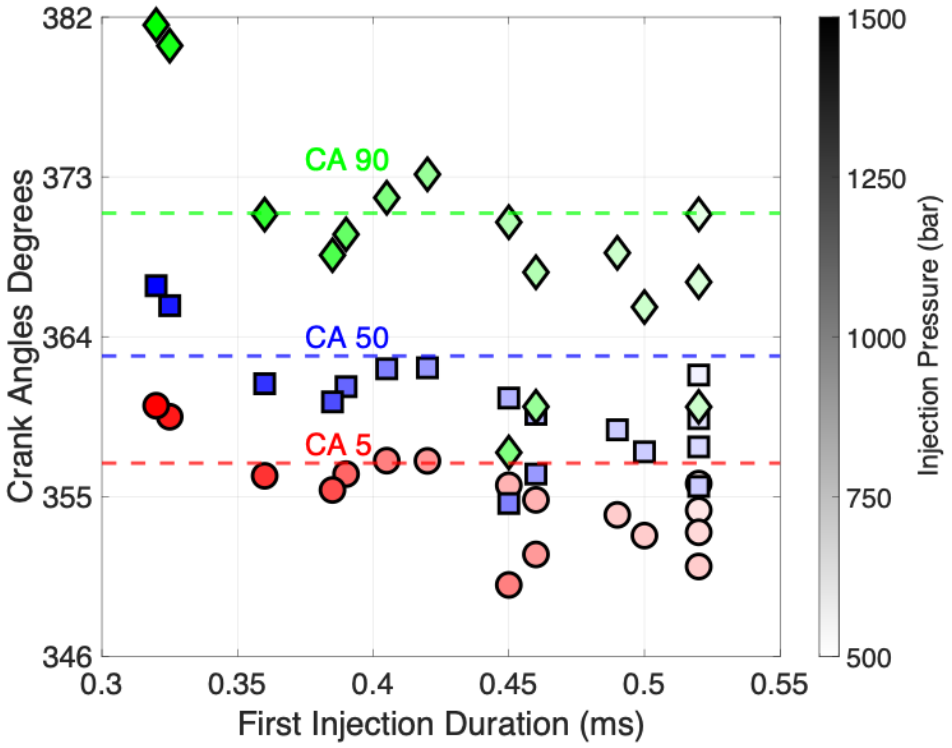

Figure 7: The trends of CA5 (circles), CA50 (squares), and CA90 (diamonds) over the first injection duration of diesel fuel (for OP#6 – OP#22) and the dotted line corresponds to the CA5, CA50, and CA90 of the reference single injection case (OP#1) Additionally, the density of the shade defines the injection pressure of the OP

The COV of IMEP, shown in Figure 8a, follows the same trend as that of the CA5 and CA50; i.e., as the combustion retards, the COV of IMEP increases. However, the COV was always less than 3%, indicating that cyclic variations were minimal for all of these OPs. The maximum pressure rise rate (MPRR), shown in Figure 8b, follows the opposite trend. As CA50 is retarded, the peak pressure decreases, and the heat release get distributed for a longer duration (discussed later). The location at which the peak pressure occurs is also retarded, thus decreasing MPRR.

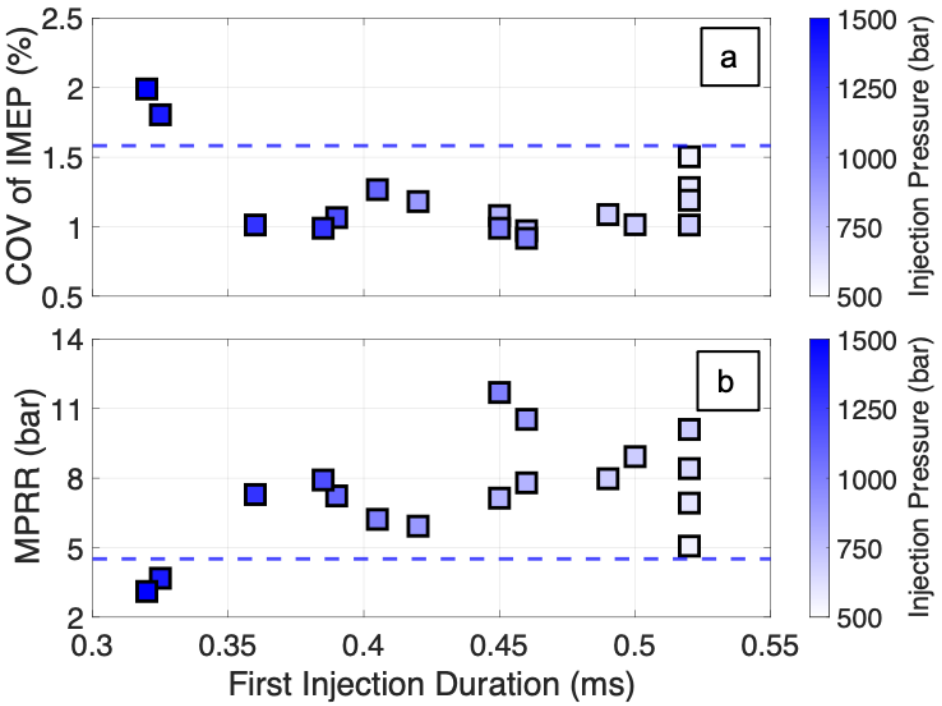

Figure 8: a) COV of IMEP, b) Maximum pressure rise rate (MPRR) over the first injection duration of diesel fuel (for OP#6 – OP#22) and the dotted line corresponds to the respective values of the reference single injection case (OP#1)

The effect of fuel injection pressure on the burn duration is shown in Figure 9. From Figure 9a, it can be seen that the burn duration trend is very similar to the CA50 trend. So, it appears that the burn duration is correlated to the combustion phasing. To verify this, burn duration is plotted against CA50 in Figure 9b, where it is seen that the burn duration increases almost linearly with the CA50. Despite this correlation between CA50 and burn duration, it may not be concluded that retarded CA50 causes longer burn durations. Rather, the calculated burn duration directly depends on CA90, which can occur later for dual injection conditions with significant heat release after the second injection (e.g., OP#22). Consequently, the correlation between CA50 and burn duration for these operating conditions is incidental (at best) and does not imply causation.

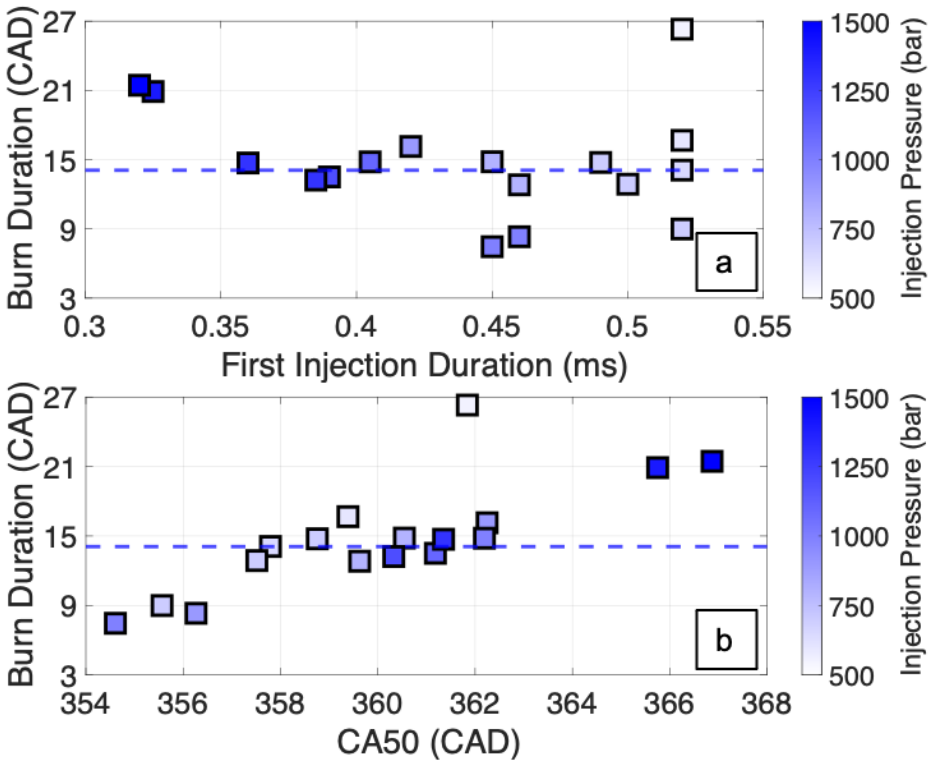

406

407 *Figure 9: a) Burn duration (CA5-90) over the first injection duration of diesel fuel and b) Burn*
408 *duration (CA5-90) over the calculated CA50 (for OP#6 – OP#22) and the dotted line corresponds*
409 *to the burn duration of the reference single injection case (OP#1)*

410 **3.2.3 Fuel Conversion Efficiency and Combustion Efficiency**

411 Indicated fuel conversion efficiency (IFCE) and combustion efficiency (η_c) for these 17
412 cases are shown in Figures 10 and 11, respectively. For any given injection duration, IFCE
413 increases slightly with increasing injection pressure. This can be explained from the CA5, CA50
414 trends, which are "more optimal" when injection pressure increases at a given injection duration.
415 Typically, for similar burn durations, a CA50 around 5 CAD after TDC leads to higher IFCE due
416 to a more optimal tradeoff between the compression work required and the expansion work
417 delivered for a given amount of fuel. In addition, combustion efficiency improvements can also
418 help improve IFCE.

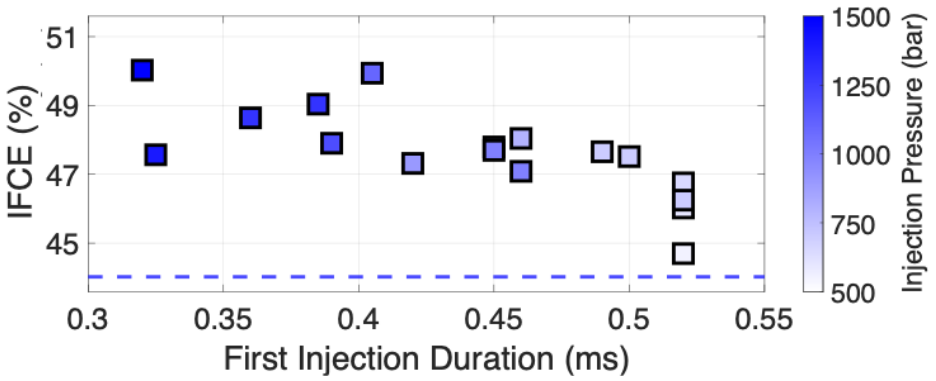

Figure 10: IFCE over the first injection duration of diesel fuel (for OP#6 – OP#22) and the dotted line corresponds to the IFCE of the reference single injection case (OP#1)

To study combustion efficiency (η_c) trends, they were plotted against three different parameters namely peak bulk temperature, CA50, and burn duration in Figures 11a, 11b, and 11c, respectively. From Figure 11a, with increasing peak bulk temperature, η_c increases for any injection pressure. An increase in bulk temperature depicts either an increase in the lowest temperature in the cylinder and/or a decrease in the fraction of volume whose temperature is too low to have complete combustion (mostly near-wall regions). Additionally, for any OPs with comparable peak bulk temperatures, the OP with higher injection pressure resulted in higher η_c. This can be attributed to the fact that higher injection pressure increase spray momentum, thus increasing entrainment rates of the surrounding methane-air mixture, and leading to more effective consumption of methane. The red dotted line represents the reference temperature of 1500 K [49] below which the oxidation of CO to CO_2 is necessarily incomplete.

Even though increasing injection pressure increases combustion efficiency, it is evident from Fig. 11 that the two cases with the highest injection pressure have the lowest η_c. It is mainly because of the later combustion phasing, longer burn durations and lower peak bulk temperatures, with all three parameters contributing to the η_c reductions. In general, η_c decreases when

combustion phasing is delayed (away from TDC) and combustion duration is relatively long, thereby reducing in-cylinder bulk gas temperatures. When combustion phasing is retarded, the instantaneous piston speed increases as the piston descends, resulting in a more rapid decrease of in-cylinder temperatures during the later combustion stages. As temperature decreases, the oxidation process gets hindered, resulting in higher unburned hydrocarbon and CO emissions, which decrease η_c.

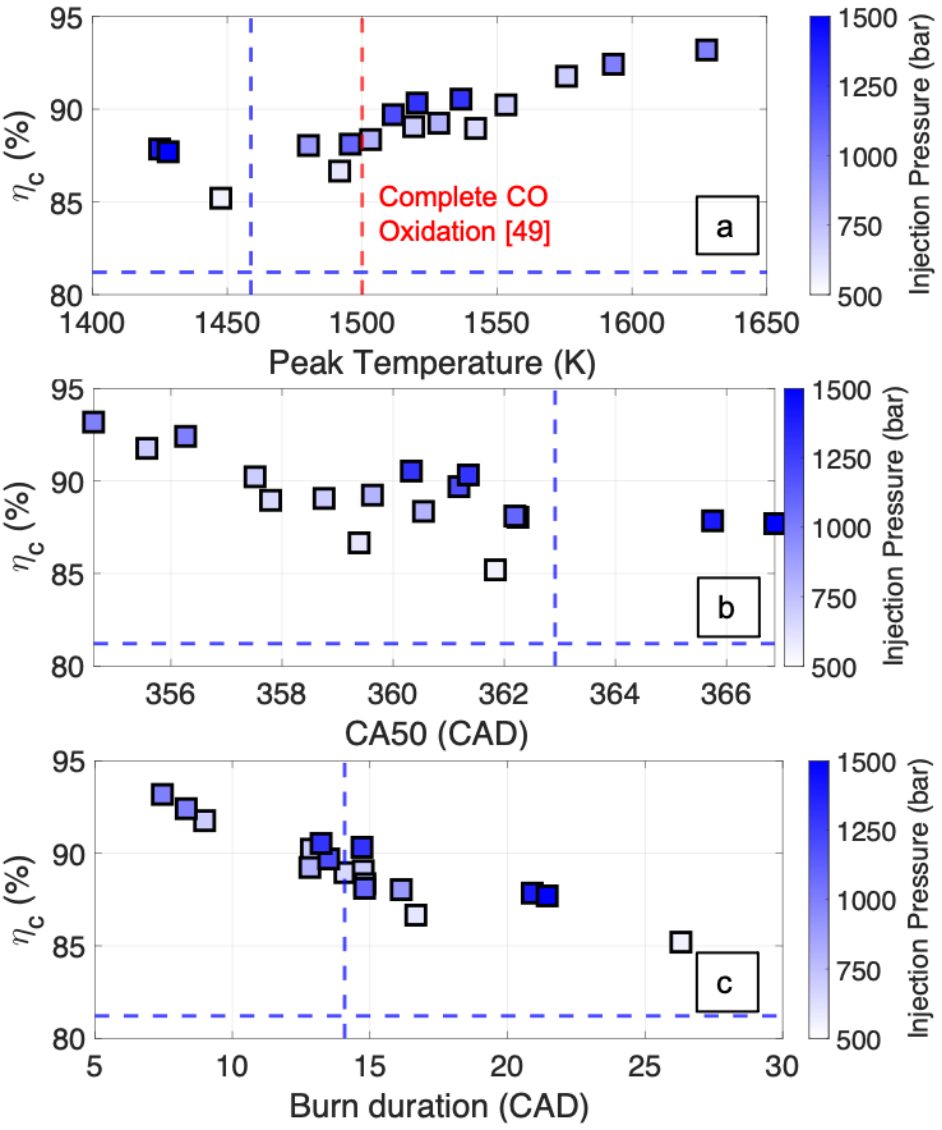

Figure 11: Combustion Efficiency (η_c) vs Peak bulk temperature, b) Combustion Efficiency vs CA50, and c) Combustion Efficiency vs Burn duration (CA5-90) (for OP#6 – OP#22), the blue

dotted line corresponds to the η_c of the reference single injection case (OP#1) and the red dotted line in Figure 11a corresponds to the minimum temperature required to oxidize CO [49]

3.2.4 Residence time and its effect on emissions

In addition to combustion phasing, combustion duration, and in-cylinder peak bulk gas temperatures, the duration for which high temperatures persist is important vis-à-vis CO and HC oxidation. In the present work, residence time (τ_{res}) is defined as the duration in CAD for which the in-cylinder bulk gas temperature stays above the threshold of 1400 K. The threshold is set to be $T_{threshold}$ = 1400 K, instead of 1500 K (below which the oxidation of CO to CO_2 is necessarily incomplete [49]) since a few operating points never reached 1500 K peak bulk gas temperature. Figure 12 shows the residence time (for reference, residence times with both $T_{threshold}$ = 1400 K and $T_{threshold}$ = 1500 K are shown), combustion duration, CAD location of the peak bulk temperature, and the start and end of the second injection of diesel. It is evident from the CAD location of the peak bulk temperature and the residence time data bars that the CAD duration between $T_{threshold}$ = 1400 K and the peak temperature is shorter compared to the CAD duration from peak temperature down to $T_{threshold}$ = 1400 K (during expansion); i.e., the bulk temperature is not symmetric about its peak location.

The peak bulk temperature does not necessarily occur at or around CA50. For some OPs (notably OP#9, #15, and #16) it happens well after CA90, due to the very early start of combustion and combustion phasing and short combustion durations. For those three OPs, although the CA90 happens before TDC, and the peak bulk temperature happens just after TDC, they are the earliest to reach the threshold temperature (due to early combustion phasings) and the latest to fall below the threshold temperature (due to high peak bulk gas temperatures) resulting in the longest residence times.

The two OPs with the highest injection pressure were the two OPs with the latest combustion phasing as discussed earlier. From Figure 12, it is seen that the start and the end of the second injection also happen during the combustion process (before CA90). From Table 3, it is clear that the ratio between the first and second injection durations is lowest for OP#21 and 22 (approximately 1). As the fraction of the overall fuel injected during the first injection is decreased, the start of combustion is retarded. Due to the later start of combustion (CA5 ~ 358 CAD), the second injection happens before the end of the heat release rate arising due to the first injection, resulting in a comparably higher second heat release rate (see Figure 6). Thus, the CA50 and CA90 are delayed for these two cases. Due to their latest combustion phasing, they had the lowest peak bulk temperatures and shortest residence times.

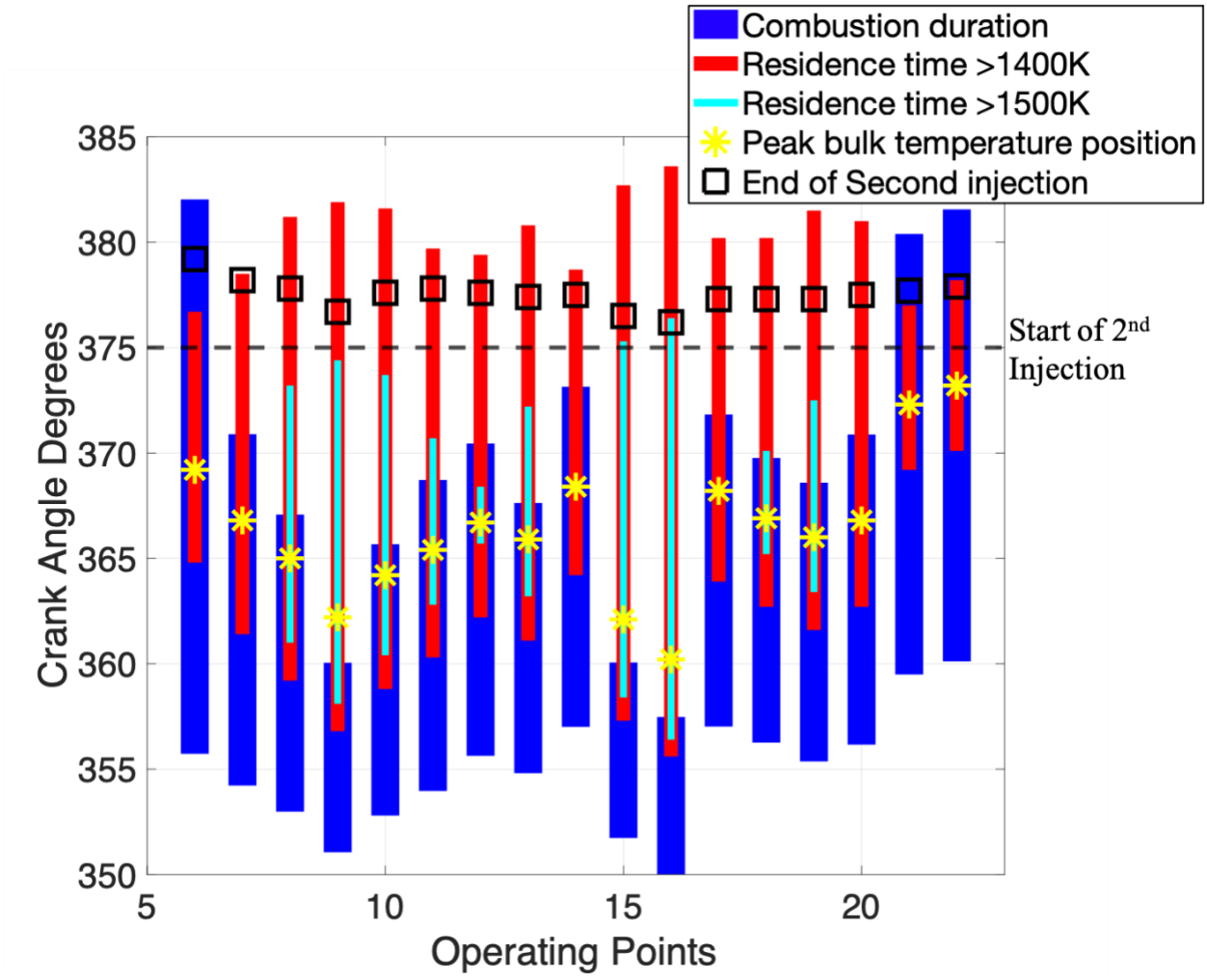

Figure 12:Combustion duration, residence time, and CAD location of peak bulk gas temperature for different operating points. Red and cyan bar represent the residence time for which the bulk temperature stays above 1400 K and 1500 K respectively, the blue bar represents the combustion duration (from CA5 to CA90) for OP#6 – OP#22. The CADs of peak bulk temperature, start and end of the second injection are also marked on the plot for reference

As discussed before, the residence time is important due to its direct impact on engine-out emissions such as CO and HC. The indicated specific emissions of CO and HC are shown in Figures 13a and 13b, respectively. Excluding OP#21 and OP#22, both emissions exhibited very similar trends in that as the residence time increases, both CO and HC emissions decrease by approximately 60%. This is because the higher residence time provides a longer duration for both HC and CO oxidation. For any given residence time, higher injection pressures resulted in lower

emissions, agreeing with other results in the literature [50 – 52]. The ISHC emissions for the dual injection OPs were always lower compared to the single injection OP, validating the original hypothesis that the second diesel injection after TDC would help improve the ISHC emissions. ISCO emissions also have a very similar trend, however, OP#6, OP#21, and OP#22 have slightly higher ISCO emissions. Another interesting trend is that the lower ISHC emissions occur at the highest injection pressures (OP#21 and OP#22), unlike ISCO emissions, despite the very short residence times for OP#21 and OP#22. The main reason for the decrease in HC emissions is the longer combustion durations for OP#21 and OP#22. However, since the combustion phasing is significantly delayed (CA90 occurs around 380 CAD), complete oxidation of HC into CO_2 is impeded, resulting in higher CO emissions. It is also important to notice those two points have the lowest peak bulk temperatures (see Fig 11), which also adversely affect CO oxidation.

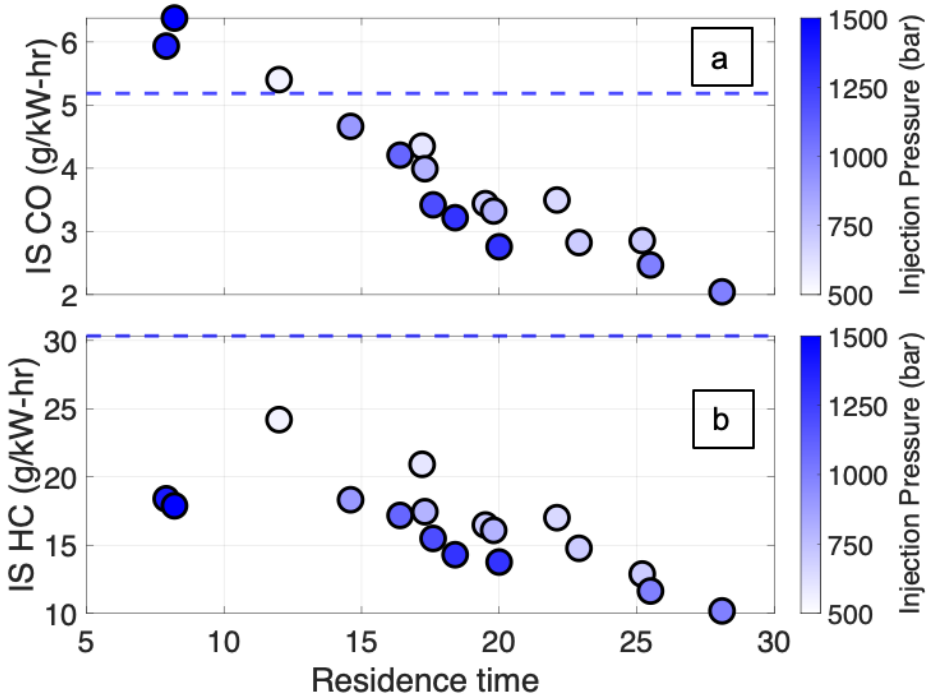

Figure 13: The effect of residence time on a) Indicated specific carbon monoxide emissions and b) Indicated specific hydrocarbon emissions. The dotted line corresponds to the corresponding indicated specific emissions of the reference single injection case (OP#1)

3.2.5 Efficiency-Emissions Tradeoffs for Different P_{rail} and Injection Duration

Both efficiency and emissions are important when considering the overall attractiveness of advanced combustion concepts. The tradeoff plots shown in Figure 14 help determine the best operating points (for the conditions examined) both in terms of emissions and efficiency. The indicated specific emissions for CO, HC, NOx, and CO_2 are plotted against IFCE. At the outset, it is evident that the IFCE of all the cases is better than the reference single injection case and there is no significant overall trend between any emissions and the efficiency. From the four subplots, four specific operating points whose IFCE were higher than 48.5% could be considered "best operating points". Ideally, the two operating points with 50% efficiency may be desirable; however, unfortunately those operating points also have significantly higher CO emissions (twice as much) and slightly higher HC emissions (20% higher) compared to the two operating points

around the IFCE of 49%. So, OP#19 and OP#20 appear to provide the best tradeoffs with respect to both efficiency and emissions. They have the lowest CO, HC, and NOx emissions. These points also have slightly higher CO_2 emissions compared to the reference single injection case; however, this is due to higher IFCE and combustion efficiency values, both of which are positive outcomes. Similarly, OP#19 and OP#20 also show approximately 11% improvement in the IFCE compared to the reference single injection operating point.

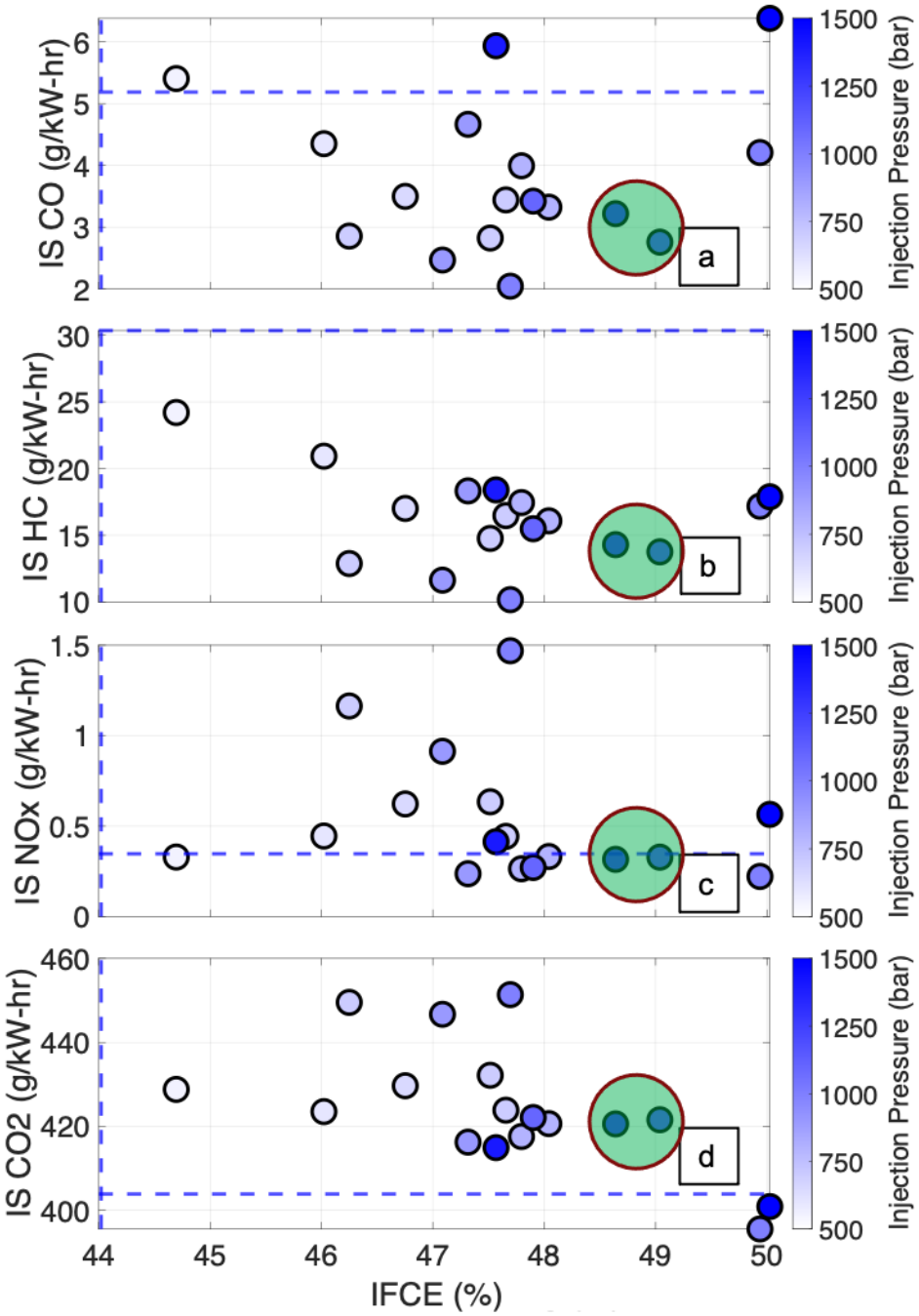

Figure 14: Efficiency-Emissions trade-off; IFCE has been plotted against a) Indicated specific carbon monoxide, b) Indicated specific hydrocarbon, c) Indicated specific oxides of nitrogen, and d) Indicated specific carbon dioxide and the dotted line represents the corresponding indicated specific emissions and indicated FC efficiency of the reference single injection case (OP#1); The most attractive operating points based on the tradeoff plots are encircled

Concerns with high smoke emissions led to the consideration of higher injection pressures with dual injection. Filter smoke number (FSN) measurements from the smoke meter for all the 17 operating points along with the reference OP#1 are shown in Figure 15. As expected, smoke emissions decreased significantly with the increase in the injection pressure. It is also interesting to note that smoke emissions for OP#19 and OP#20 with dual injection matched the smoke emissions of the reference single injection case along with an 11% increase in IFCE (compared to 44% IFCE of reference case) and ~40% lower ISCO and ~50% lower ISHC emissions. Consequently, it is reasonable to conclude that OP#19 and OP#20 are the most optimal operating conditions vis-à-vis efficiency-emissions tradeoffs.

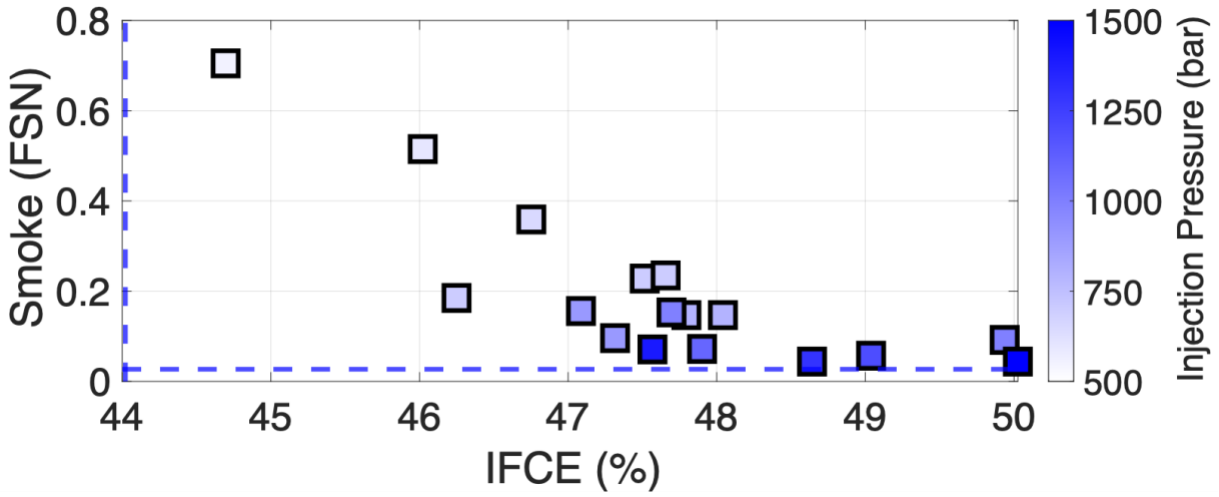

Figure 15: Smoke emissions of the OP#6 to #22 and the dotted line represents the corresponding smoke meter measurements and IFCE for the reference single injection case (OP#1)

4. CONCLUSIONS

Advantages of a second diesel injection in diesel-methane dual-fuel low temperature combustion (LTC) were explored with the specific goals of improving IFCE, η_c, and reducing HC and CO emissions without significantly compromising the inherent NOx and smoke benefits of dual fuel LTC. The study was conducted on a single-cylinder research engine with the following fixed operating conditions: intake pressure of 1.5 bar, engine speed of 1500 rpm, and BMEP of 5 bar. After exploring 22 different operating conditions (1 single injection and 21 different combinations of double diesel injections at various diesel injection pressures), the following conclusions were attained. The single diesel injection case with an injection timing of 310 CAD, diesel injection pressure of 500 bar, and a methane percentage energy substitution (PES) of 85 % was considered as the reference condition for the following conclusions.

a) Close-coupled dual diesel injections (SOI1 = 310 CAD and SOI2 = 320 CAD and 325 CAD) resulted in earlier combustion phasing (CA50 advanced by ~7 CAD) due to high stratification, a 5% improvement in combustion efficiency, a 10% increase in peak cylinder pressure, and 6 times higher NOx emissions, compared to the single injection operating point (Baseline values: CA50 = 363 CAD, combustion efficiency = 81%, peak cylinder pressure = 107 bar, ISNOx = 0.35 g/kWh).

b) Keeping all other operating parameters fixed, when the second SOI was retarded past TDC and a significant dwell was ensured between the first and the second diesel injections (~ 65 CAD), the smoke emissions increased significantly from 0.027 FSN for the reference single injection case to 0.825 FSN, although the NOx emissions and IFCE were similar to the single injection values.

c) Significant improvements were achieved in efficiency-emissions tradeoffs by increasing the injection pressure to 1000 bar (and higher).

   i. Decreasing the first injection duration (and the amount of fuel injected with the first injection) retards the start of combustion and the combustion phasing since the second injection occurs well past CA50 (in some cases even after CA90) and has little impact on the combustion energy release rates.

   ii. Fuel conversion efficiency increased steadily with injection pressure. The maximum efficiency achieved was ~50% (14% increase from the single injection case of 44% IFCE)

d) The most attractive operating points were found to be the OP#19 and OP#20, with the injection pressure of 1200 bar and 1300 bar, respectively, at 75% PES, SOI1 = 310 CAD and SOI2 = 375 CAD since these two operating points exhibited ~ 11% improvement in IFCE, the same ISNOx emissions, 40% and 50% reduction in ISCO and ISHC emissions, respectively, compared to the reference single injection case.

5. ACKNOWLEDGMENTS

The authors gratefully acknowledge financial support from the Alliance for Sustainable Energy, LLC (RFP Number RHQ-8-82305) and from the Alabama Transportation Institute (for DH). The authors acknowledge Mr. Vijayaraghavan Sridhar and Ms. Yamini Baskara Babu for their efforts in developing the MATLAB-based chemical equilibrium code used in a part of this analysis.

REFERENCES

1. Yao, M., Zheng, Z., Liu, H., (2009) “Progress and recent trends in homogeneous charge compression ignition (HCCI) engines.” Progress in Energy and Combustion Science, 25, 398-437.
2. Noehre, C., Andersson, M., Johansson, B., Hultqvist, A., (2006) “Characterization of partially premixed combustion.” SAE Technical Paper 2006-01-3412.
3. Musculus, M.P.B., Miles, P.C., Pickett, L.M., (2013) “Conceptual models for partially premixed low-temperature diesel combustion,” Progress in Energy and Combustion Science, 39, 246-283.
4. Kalghatgi, G.T., Risberg, P., Angstrom, H.-E., (2007) “Partially pre-mixed auto-ignition of gasoline to attain low smoke and low NOx at high load in a compression ignition engine and comparison with a diesel fuel.” SAE Technical Paper 2007-01-0006.
5. Ciatti, S.A., Subramanian, S., (2011) “An experimental investigation of low-octane gasoline in diesel engines.” Trans. ASME: Journal of Engineering for Gas Turbines and Power, 133(9), 092802, doi:10.1115/1.4002915
6. Lawler, B., Splitter, D., Szybist, J., & Kaul, B. (2017). Thermally Stratified Compression Ignition: A new advanced low temperature combustion mode with load flexibility. Applied energy, 189, 122-132.
7. Gainey, B., Hariharan, D., Yan, Z., Zilg, S., Rahimi Boldaji, M., & Lawler, B. (2018). A split injection of wet ethanol to enable thermally stratified compression ignition. International Journal of Engine Research, 1468087418810587.

8. Krishnan, S.R., Srinivasan, K.K., Singh, S., Bell, S.R., Midkiff, K.C., Gong, W., Fiveland, S.B., Willi, M., (2004) "Strategies for Reduced NOx Emissions in Pilot-Ignited Natural Gas Engines." Trans. ASME: Journal of Engineering for Gas Turbines and Power, 126, 665-671.
9. Srinivasan, K.K., Krishnan, S.R., Singh, S., Midkiff, K.C., Bell, S.R., Gong, W., Fiveland, S.B., Willi, M. (2006) "The Advanced Injection Low Pilot Ignited Natural Gas Engine: A Combustion Analysis." ASME Journal of Engineering for Gas Turbines and Power, Vol. 128, 213-218.
10. Azimov, U., Tomita, E., Kawahara, N., Harada, Y., (2011) "Premixed mixture ignition in the end-gas region (PREMIER) combustion in a natural gas dual-fuel engine: operating range and exhaust emissions." International Journal of Engine Research, 12, 484-497.
11. Li, W., Liu, Z., Wang, Z., (2016) "Experimental analysis and theoretical analysis of the combustion process at low loads of a diesel natural gas dual-fuel engine." Energy, 94, 728-741.
12. Kokjohn, S.L., Hanson, R.M., Splitter, D.A., Reitz, R.D., (2011) "Fuel reactivity controlled compression ignition (RCCI): A pathway to controlled high-efficiency clean combustion." International Journal of Engine Research, 12(3), 209–226.
13. Kokjohn SL, Hanson RM, Splitter DA, Reitz RD. Experiments and modeling of dualfuel HCCI and PCCI combustion using in-cylinder fuel blending. SAE Int J Engines 2010;2(2):24–39.
14. Curran S, Prikhodko V, Cho K, Sluder CS, Parks J, Wagner R, et al. In-cylinder fuel blending of gasoline/diesel for improved efficiency and lowest possible emissions on a multi-cylinder light-duty diesel engine (No. 2010-01-2206). SAE Technical Paper; 2010.

15. Reitz RD. High efficiency fuel reactivity-controlled compression ignition (RCCI) combustion. Directions in engine efficiency and emissions research conference, Detroit, MI, Sept. 2010. p. 27–30.
16. Elliot, M.A., Davis, R.F. (1951) "Dual-fuel combustion in diesel engines," Industrial and Engineering Chemistry, 43 (12), 2854-2864.
17. Felt, A.E., Steele, W.A., Jr. (1962) "Combustion control in dual-fuel engines," Transactions of the Society of Automotive Engineers, 70, 644-653.
18. Karim, G.A., Khan, M.O. (1968) "Examination of effective rates of combustion heat release in a dual-fuel engine," Proceedings of the Institution of Mechanical Engineers: Journal of Mechanical Engineering Science, 10(1), 13-23.
19. Karim, G.A. (1980) "A review of combustion processes in the dual fuel engine – the gas diesel engine," Progress in Energy and Combustion Science, 6, 277-285.
20. Doughty, G.E., Bell, S.R., Midkiff, K.C. (1992). "Natural gas fueling of a Caterpillar 3406 diesel engine." Trans. ASME: Journal of Engineering for Gas Turbines and Power, 114, 459-465.
21. Selim, M.Y.E. (2005). "Effect of engine parameters and gaseous fuel type on the cyclic variability of dual fuel engines." Fuel, 84, 961-971.
22. Carlucci, A.P., de Risi, A., Laforgia, D., Naccarato, F. (2008) "Experimental investigation and combustion analysis of a direct injection dual-fuel diesel-natural gas engine." Energy, 33, 256-263.
23. Sahoo, B.B., Sahoo, N., Saha, U.K., (2009) "Effect of engine parameters and type of gaseous fuel on the performance of dual-fuel gas diesel engines – A review." Renewable and Sustainable Energy Reviews, 13, 1151-1184.

649 24. Korakianitis, T., Namasivayam, A.M., Crookes, R.J. (2011) “Natural-gas fueled spark-ignition
650 (SI) and compression-ignition (CI) engine performance and emissions,” Progress in Energy
651 and Combustion Science, 37(1), 89-112. doi: 10.1016/j.pecs.2010.04.002
652 25. Lounici, M.S., Loubar, K., Tarabet, L., Balistrou, M., Niculescu, D.-C., Tazerout, M., (2014)
653 “Towards improvement of natural gas-diesel dual fuel mode: An experimental investigation
654 on performance and exhaust emissions.” Energy, 64, 200-211.
655 26. Tarabet, L., Loubar, K., Lounici, M.S., Khiari, K., Belmrabet, T., Tazerout, M., (2014)
656 “Experimental investigation of DI diesel engine operating with eucalyptus biodiesel/natural
657 gas under dual fuel mode.” Fuel, 133, 129-138. doi:10.1016/j.fuel.2014.05.008
658 27. Wei, L., Geng, P., (2016) “A review of natural gas/diesel dual fuel combustion, emissions and
659 performance.” Fuel Processing Technology, 142, 264-278.
660 28. Krishnan, S.R., Biruduganti, M., Mo, Y., Bell, S.R., Midkiff K.C. (2002). “Performance and
661 heat release analysis of a pilot-ignited natural gas engine.” International Journal of Engine
662 Research, 3(3), 171-184.
663 29. Papagiannakis, R.G., Hountalas, D.T. (2003) “Experimental Investigation Concerning The
664 Effect of Natural Gas Percentage on Performance and Emissions of a DI Dual Fuel Diesel
665 Engine” Applied Thermal Engineering, 23, 353-365.
666 30. Karim, G.A., (2003) “Combustion in Gas Fueled Compression: Ignition Engines of the Dual
667 Fuel Type.” Trans. ASME: Journal of Engineering for Gas Turbines and Power, 125, 827-836.
668 31. Papagiannakis, R.G., Rakopoulos, C.D., Hountalas, D.T., Rakopoulos, D.C. (2010) “Emission
669 characteristics of high speed, dual fuel, compression ignition engine operating in a wide range
670 of natural gas/diesel fuel proportions.” Fuel, 89(7), 1397-1406.

671 32. Dec, J.E., (1997) “A Conceptual Model of DI Diesel Combustion Based on Laser-Sheet
672 Imaging.” SAE Technical Paper 970873.
673 33. Raihan, M. S., Guerry, E. S., Dwivedi, U., Srinivasan, K. K., & Krishnan, S. R. (2015).
674 Experimental analysis of diesel-ignited methane dual-fuel low-temperature combustion in a
675 single-cylinder diesel engine. Journal of Energy Engineering, 141(2), C4014007.
676 34. Guerry, E. S., Raihan, M. S., Srinivasan, K. K., Krishnan, S. R., & Sohail, A. (2016). Injection
677 timing effects on partially premixed diesel–methane dual fuel low temperature
678 combustion. Applied energy, 162, 99-113.
679 35. Carlucci, A. P., Ficarella, A., Laforgia, D., & Strafella, L. (2017). Improvement of dual-fuel
680 biodiesel-producer gas engine performance acting on biodiesel injection parameters and
681 strategy. Fuel, 209, 754-768.
682 36. Yadav, J., & Ramesh, A. (2018). Comparison of single and multiple injection strategies in a
683 butanol diesel dual fuel engine. Journal of Energy Resources Technology, 140(7).
684 37. Yadav, J., & Ramesh, A. (2018). Injection strategies for reducing smoke and improving the
685 performance of a butanol-diesel common rail dual fuel engine. Applied energy, 212, 1-12.
686 38. Huang, H., Zhu, Z., Chen, Y., Chen, Y., Lv, D., Zhu, J., & Ouyang, T. (2019). Experimental
687 and numerical study of multiple injection effects on combustion and emission characteristics
688 of natural gas–diesel dual-fuel engine. Energy Conversion and Management, 183, 84-96.
689 39. Bartolucci, L., Cordiner, S., Mulone, V., Krishnan, S. R., & Srinivasan, K. K. (2021). A
690 Computational Investigation of the Impact of Multiple Injection Strategies on Combustion
691 Efficiency in Diesel–Natural Gas Dual-Fuel Low-Temperature Combustion Engines. Journal
692 of Energy Resources Technology, 143(2).

40. Ma, S., Zheng, Z., Liu, H., Zhang, Q., & Yao, M. (2013). Experimental investigation of the effects of diesel injection strategy on gasoline/diesel dual-fuel combustion. Applied Energy, 109, 202-212.
41. Diesel Engine Emission Measurement Procedure - J1003_200210, SAE International, 2002: also available at https://www.ecfr.gov/cgi-bin/text-idx?SID=1c4269ace85c6e3b049a593bcd9fe44b&mc=true&node=pt40.21.86&rgn=div5#se40.21.86_1144_694
42. Aamir Sohail (2015), An experimental investigation of dual-injection strategies on diesel-methane dual-fuel low temperature combustion in a Single Cylinder Research Engine, MS thesis, Mississippi State University
43. Heywood, J.B. (1988) Internal Combustion Engine Fundamentals, McGraw-Hill, New York.
44. McBride, B. J. (1993). Coefficients for calculating thermodynamic and transport properties of individual species (Vol. 4513). NASA Langley Research Center.
45. Engelmayer, M., Wimmer, A., Taucher, G., Hirschl, G., & Kammerdiener, T. (2015). Impact of very high injection pressure on soot emissions of medium speed large diesel engines. Journal of engineering for gas turbines and power, 137(10).
46. Tao, F., Liu, Y., RempelEwert, B. H., Foster, D. E., Reitz, R. D., Choi, D., & Miles, P. C. (2005). Modeling the effects of EGR and injection pressure on soot formation in a high-speed direct-injection (HSDI) diesel engine using a multi-step phenomenological soot model. SAE transactions, 263-283.
47. Patterson, M. A., Kong, S. C., Hampson, G. J., & Reitz, R. D. (1994). Modeling the effects of fuel injection characteristics on diesel engine soot and NOx emissions. SAE transactions, 836-852.

716 48. Yokota, H., Kamimoto, T., Kosaka, H., & Tsujimura, K. (1991). Fast burning and reduced soot
717 formation via ultra-high pressure diesel fuel injection (No. 910225). SAE Technical Paper.
718 49. Sjöberg, M. and Dec, J.E., "An Investigation into Lowest Acceptable Combustion
719 Temperatures for Hydrocarbon Fuels in HCCI Engines," Proceedings of the Combustion
720 Institute 30(2):2719-2726, 2005.
721 50. Pierpont, D. A., & Reitz, R. D. (1995). Effects of injection pressure and nozzle geometry on
722 DI diesel emissions and performance. SAE transactions, 1041-1050.
723 51. İçıngür, Y., & Altiparmak, D. (2003). Effect of fuel cetane number and injection pressure on a
724 DI Diesel engine performance and emissions. Energy conversion and management, 44(3), 389-
725 397.
726 52. Liu, J., Yao, A., & Yao, C. (2015). Effects of diesel injection pressure on the performance and
727 emissions of a HD common-rail diesel engine fueled with diesel/methanol dual fuel. Fuel, 140,
728 192-200.